Petroleum Science 23 (2026) 1220–1232

Contents lists available at ScienceDirect

Petroleum Science

journal homepage: www.keaipublishing.com/en/journals/petroleum-science

Original Paper

Lateral constrained multi-trace seismic inversion based on deep learning

Jian Zhang [a,b,c], Yi-Ran Xue [a,c], Xiao-Yan Zhao [a,c,*], Jing-Ye Li [b]

[a] The Faculty of Geosciences and Engineering, Southwest Jiaotong University, Chengdu, 611756, Sichuan, China
[b] National Key Laboratory of Petroleum Resources and Engineering, China University of Petroleum (Beijing), Beijing, 102249, China
[c] Sichuan Province Engineering Technology Research Center of Ecological Mitigation of Geohazards in Tibet Plateau Transportation Corridors, Chengdu, 611756, Sichuan, China

ARTICLE INFO

Article history:
Received 21 April 2025
Received in revised form
8 November 2025
Accepted 5 December 2025
Available online 9 December 2025

Edited by Meng-Jiao Zhou

Keywords:
Seismic inversion
Multi-trace constraints
Deep learning
Physics-guided strategy

ABSTRACT

Seismic inversion is a widely used method for exploring and characterizing subsurface geological structures, especially in the context of oil and gas exploration. The data-driven approach exemplified by deep learning (DL) circumvents the need for pre-defined physical system and is used to solve seismic inversion problems. However, the DL-based inversion method is sensitive to noise and is typically performed trace-by-trace. When the inversion results are aggregated into a 2D image, the lateral continuity of the final output is often inadequate, impacting subsequent interpretation and evaluation. In contrast, conventional DL-based multi-trace seismic inversion typically treats multi-trace seismic data as input without fully accounting for the coupling relationships between neighboring traces. Therefore, we propose a lateral constrained multi-trace seismic inversion method based on DL to enhance the continuity and geological reliability of the inversion results. Given the similarities among neighboring traces, the method employs adjacent multi-trace seismic data as input to the network and designs multi-trace coupling constraints to ensure the lateral consistency of the prediction outcomes. Moreover, physical laws and low-frequency prior information are incorporated into the network training process to mitigate the dependence of data-driven methods on large amounts of training data. The effectiveness of the proposed method in enhancing both the lateral continuity and accuracy of inversion results is demonstrated by applying it to synthetic and real datasets, and comparing the results with those of conventional DL-based single-trace and multi-trace inversion methods.

1. Introduction

Seismic inversion is a powerful technique for deriving elastic parameters such as impedance, velocity, and density, which are crucial for informing and enhancing subsequent reservoir interpretation and characterization (Bosch et al., 2010; Delépine et al., 2011; Pendrel, 2001; Veeken and Da Silva, 2004). Seismic inversion, from a mathematical perspective, is usually ill-posed, meaning that several distinct subsurface models may fit the same observed seismic data (Ahmed et al., 2024; Huang et al., 2020; Lin et al., 2023). Moreover, seismic inversions are often highly nonlinear, further complicating the solution process (Chen et al., 2020; Grana et al., 2022; Wang et al., 2022; Zhou et al., 2020). To address these challenges, it is typically necessary to define an objective function based on the known physical system (i.e., the relationship between elastic parameters and seismic data). Optimization techniques (e.g., newton iteration, conjugate gradient, and global search) are then employed to minimize the objective function's error, leading to the desired solution (Gao et al., 2020; Ha and Marfurt, 2017; Shi et al., 2024; Zhang et al., 2021b). However, the complexity and inhomogeneity of the subsurface make the relationship between seismic data and elastic variables intricate, complicating efforts to accurately express this connection. Additionally, solving nonlinear problems is both challenging and time-consuming. To address these issues, scholars are increasingly turning to data-driven seismic inversion methods, which enable a more nuanced understanding of subsurface properties by leveraging patterns and correlations within the data. Deep learning (DL), a quintessential example of a data-driven

* Corresponding author.
E-mail address: xyzhao2@swjtu.edu.cn (X.-Y. Zhao).
Peer review under the responsibility of China University of Petroleum (Beijing).

https://doi.org/10.1016/j.petsci.2025.12.010

approach, has gained increasing popularity in recent years and is widely applied across various industries because of its outstanding ability to uncover complex patterns and relationships in large datasets. This capability has made it an especially favored method for enhancing the accuracy of seismic inversion (Chen et al., 2024; Mousavi and Beroza, 2022; Zhang et al., 2021a, 2021c).

DL-based seismic inversion does not rely on a predefined physical system. Instead, it leverages statistical theory to directly convert seismic data into subsurface elastic parameters, guided by provided training datasets. As early as the last century, scholars utilize fully connected neural networks to achieve direct mapping of seismic data to 1D velocities, attaining a tested accuracy of nearly 80% (Röth and Tarantola, 1994). This success highlights the capability of neural networks to address complex nonlinear inverse problems. In recent years, the rapid advancement in computing power and related algorithms has enabled the development of neural networks with more hidden layers. These networks can extract richer and more sophisticated features, thereby significantly enhancing the reliability of inversion results. Convolutional Neural Networks (CNNs) have also greatly benefited from these advancements, demonstrating their powerful capabilities. By mimicking the human visual system, CNNs use layers of abstraction and feature extraction to efficiently reduce the dimensionality of large datasets without compromising the integrity of the information. This process enables the effective processing and recognition of complex data. As a result, CNNs have become one of the most widely used and effective models in fields such as image processing, speech recognition, and natural language processing.

Inspired by these advancements, geophysicists recognize the similarity between seismic inversion and these tasks, and consequently apply CNNs to seismic exploration. Das et al. (2019) designed a two-layer CNN to map seismic data to impedance and successfully train the network using synthetic data. Zheng et al. (2019) utilized and trained a CNN to predict 1D velocity and density profiles from input seismic data. Mustafa and AlRegib (2020) simultaneously trained two CNNs on different datasets and imposed a soft constraint on the weight similarity between them, enabling mutual learning where beneficial to improve generalization performance on their respective datasets. Wu et al. (2021) improved the 1D network by developing a 2D CNN and integrating the constraints of an initial impedance model, which resulted in more stable impedance predictions. Aleardi and Salusti (2021) used the discrete cosine transform re-parameterization method to preprocess the seismic data and then fed it into a CNN to achieve predictions of velocity and density. Zhang et al. (2021c) performed seismic inversion using a network that combined a CNN with a fully connected neural network (FCNN). This approach introduces an initial model alongside the input seismic data, enhancing the robustness of the predictions and the generalization ability of the network. Furthermore, the method employs a transfer learning strategy to fine-tune the network, initially trained on synthetic data, using limited well-log data, which facilitates the application of deep learning methods to real-world scenarios. Cao et al. (2022) generated sufficiently diverse datasets for pre-stack seismic inversion using limited well data and seismic data, and introduced reflection coefficient constraints in a CNN-based U-Net network to improve prediction accuracy. Zhang et al. (2023) proposed an initial model-constrained loss function term in CNN-based seismic inversion, achieving laterally continuous elastic parameter inversion results under various signal-to-noise ratio conditions. Dodda et al. (2023) trained an attention-based deep convolutional neural network (ADCNN) using supervised learning with predefined acoustic impedance and subsequently updated the ADCNN in an unsupervised manner by incorporating the physics of the forward problem. Considering that CNNs primarily focus on extracting spatial attributes from input data and may overlook temporal attributes, scholars have introduced recurrent neural networks (RNNs) to complement CNNs, addressing the limitations of using CNNs alone (Guo et al., 2019; Song et al., 2022; Zhang et al., 2022). However, all the methods mentioned above fall into the category of supervised learning, where the quality of the results heavily depends on having a large number of valid training datasets. This requirement is often at odds with the limited well-log data available in real seismic exploration.

Alternatively, physics-guided methods have created a buzz in DL-based seismic inversion by integrating physical laws to alleviate the data dependency of data-driven methods. Biswas et al. (2019) used a CNN as an inversion network, feeding its output into physical laws to generate synthetic seismic records. The inversion network is then updated using the residuals between the synthetic seismic record and the input seismic data, thereby enabling effective training of the network even with small sample sizes. Zou et al. (2023) used a semi-supervised network combined with domain adversarial and spatial fusion strategies to reduce the network's dependence on labels and achieve seismic impedance prediction. Liu et al. (2023a) embedded seismic forward modeling at the end of the network and remapped the inversion results back to the data domain to construct a self-supervised loss-trained neural network, enhancing the network's ability to generalize to new tasks. Fernandes et al. (2024) utilized cycle-consistent CNN to ensure coherence in translating seismic data to impedance and back to the data domain, thereby achieving high-resolution impedance prediction of turbidite reservoirs. Most of these methods are executed trace-by-trace, resulting in inversion outputs with poor lateral continuity, which increases the risk of subsequent reservoir interpretation.

Inspired by model-driven multi-trace seismic inversion (Hamid and Pidlisecky, 2015; Zhou et al., 2019), some scholars have attempted to apply a similar strategy in deep learning-based seismic inversion to improve the lateral continuity of the inversion results. Wu et al. (2021) used a 2D CNN and designed an adaptive loss training method, integrating lateral structural constraints to predict a laterally more consistent impedance model. Liu et al. (2023b) used multi-trace seismic data as network input and leveraged the multi-trace information for training and prediction, thereby reducing the issue of lateral geological artifacts. Gao et al. (2024) used 2D training datasets to train a U-shaped 2D network, which captured spatially varying structures and produced more accurate impedance results compared to the 1D network. However, these existing methods simply input multi-trace seismic data into a 2D network, where 2D spatial features are automatically extracted, but the output remains 1D data, and the coupling relationship between neighboring traces of the output data is not considered. To address this issue, building on the aforementioned research, we propose a DL-based lateral constrained multi-trace seismic inversion method to enhance the continuity and geological reliability of the inversion results. The proposed method integrates the laws of physics and low-frequency information into the network training process to reduce the dependence of data-driven methods on large amounts of training data. In addition, considering the similarity between neighboring traces, the proposed method uses adjacent multi-trace seismic data as network inputs and designs multi-trace coupling constraints between the output results to improve the lateral consistency of the predictions. In this way, the proposed method can both reduce dependence on the training dataset and ensure the coupling relationship between neighboring traces of the prediction results. In this paper, the performance of the

proposed method is demonstrated through an example of post-stack seismic inversion.

The rest of this article is organized as follows. Firstly, we introduce the physics-guided deep learning seismic inversion framework, which serves as the foundation for training network and constructing multi-trace constraints. Next, based on the physics-guided loss term, we describe the construction of a loss function incorporating multi-trace lateral constraints, and provide a detailed account of the network architecture and training procedure incorporating well-log data. Then, the accuracy and advantage of the proposed method are verified through post-stack seismic impedance inversion, using both synthetic and actual data, and comparing it with traditional DL-based single- and multi-trace seismic inversion techniques. The final section offers some discussions and conclusions.

2. Methods

Given that the effectiveness of deep learning methods largely hinges on the availability of extensive training datasets, and considering the challenges in acquiring a substantial number of valid training datasets for real-world seismic surveys, this section introduces physics-guided deep learning seismic inversion techniques. These methods aim to lessen the reliance on large training datasets while maintaining or improving the accuracy of seismic inversion. Subsequently, the single-trace physics-guided deep learning seismic inversion method is extended to a multi-trace approach. Additionally, a coupled loss term between the multi-trace outputs is designed to further enhance the lateral continuity of the prediction results. Finally, the detailed architecture of the networks is presented to facilitate the reproduction of the experimental results.

2.1. Physics-guided deep learning-based seismic inversion

The goal of seismic inversion is to predict subsurface impedance models based on given seismic data. Most deep learning methods for solving inverse problems are purely data-driven. This approach heavily relies on a large number of valid training datasets, which is often not feasible in seismic inversion due to the limited availability of training data (i.e., well-log data) in seismic surveys. To address this issue, the forward modeling operator is integrated into the network to compute the error between observed and synthetic seismic data, aiding in the updating of the network. Fig. 1 demonstrates the framework of physics-guided deep learning (PGDL)-based seismic impedance inversion. The seismic data is used as input to the network to generate the output impedance. In the presence of labels, this output can be directly compared with the labels. In other cases, the output impedance of inversion network is processed by the forward modeling operator to compute the reflection coefficients (i.e., reflectivity), which are then convolved with the wavelet to generate the synthetic seismic record. This synthetic record can then be compared with the input seismic data. To ensure that predictions adhere to known physical laws while reducing the need for large labelled datasets in data-driven approaches, the objective function for the PGDL training is defined as:

$$\mathscr{L} = \underbrace{\lambda_1 \cdot ||\mathbf{m} - \mathscr{G}_\Theta(\mathbf{d}_l)||_2^2}_{\mathscr{L}_1} + \underbrace{\lambda_2 \cdot ||\mathbf{d} - F(\mathscr{G}_\Theta(\mathbf{d}))||_2^2}_{\mathscr{L}_2} \quad (1)$$

where $\mathbf{m}$ and $\mathbf{d}_l$ represent the labelled data (i.e., well-log impedance data) and their corresponding seismic data, respectively. $\mathbf{d}$ represents seismic data with or without labels. $\mathscr{G}_\Theta$ denotes the network that converts seismic data to impedance, where Θ represents the network parameters to be optimized. F denotes the known forward modeling operator that converts impedance to a seismic record. That is, the loss function of PGDL consists of two components, the model misfit term ($\mathscr{L}_1$) and the data misfit term ($\mathscr{L}_2$). The model misfit term, $\mathscr{L}_1$, assesses the difference between the predicted impedance model and the true impedance model. The data misfit term, $\mathscr{L}_2$, evaluates the differences between the observed seismic data and the synthetic seismic record obtained using the forward modeling operator. λ is a weighting factor used to balance these two misfit terms. When λ_2 is equal to 0, PGDL degenerates into a purely data-driven algorithm. When well-log data is available, PGDL can use both the model and the data to regulate the back-propagation process. Once the model is well-trained, we can use the network to estimate the unknown impedance model for a new set of measured seismic data. Impedance prediction can also be performed during the training process.

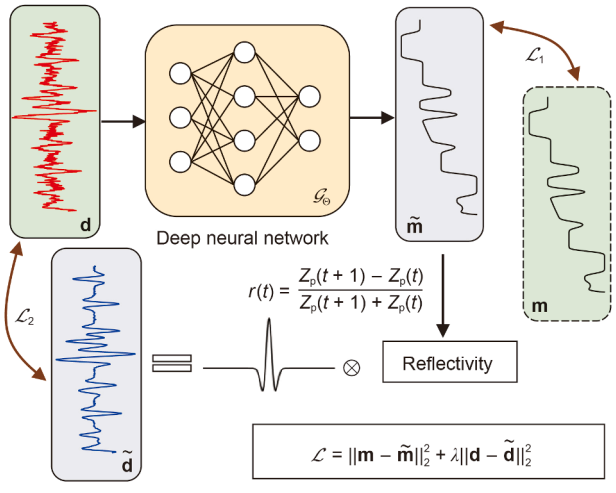

Fig. 1. An overview of the framework for physics-guided deep learning-based seismic inversion.

2.2. Lateral constrained multi-trace PGDL-based seismic inversion

The multi-trace inversion strategy helps to enhance the lateral continuity of the inversion results. However, traditional multi-trace DL-based seismic inversion typically uses multi-trace seismic data as input, but the output remains single-trace well-log data, with adjacent traces of the wells represented by zero masks. To this end, we propose a physics-guided deep learning (PGDL)-based laterally constrained multi-trace seismic inversion. This approach combines a physics-guided algorithm with a traditional multi-trace inversion strategy and designs a new lateral loss function term, as shown in Fig. 2. The proposed method inputs adjacent multi-trace seismic records, containing both labelled and unlabelled data, into the network along with an initial impedance model. The loss function design is divided into two main parts, labelled data and unlabelled data. In this paper, we use three adjacent traces of data as input. Since well-log data is typically a single trace, in the model misfit section (i.e., $Loss_1$), we only calculate the loss between the network output corresponding to the well location and the reference impedance. It is noteworthy that only a small amount of labelled data is required (green bar in the reference model in Fig. 2), and it is not necessary for the entire reference model to be known. In the unlabelled data section, we do not require known labels, so the loss in this section is applicable to

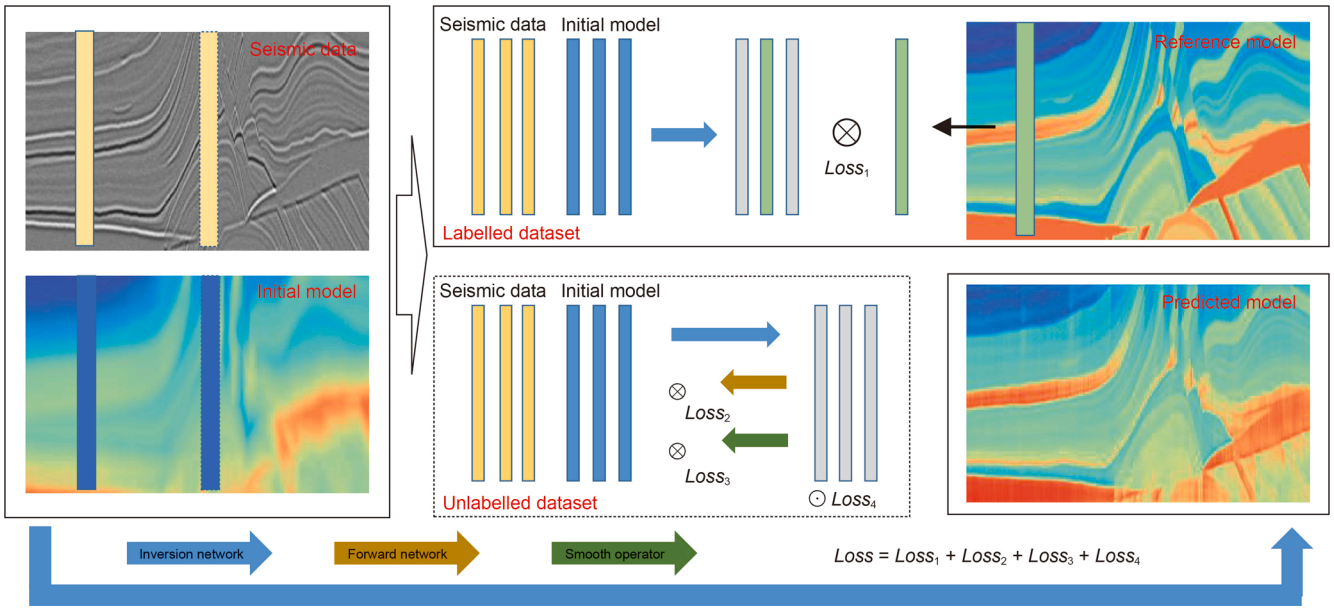

Fig. 2. An overview of the framework for lateral constrained multi-trace physics-guided deep learning-based seismic inversion.

seismic data regardless of whether it contains labels. First, the seismic data is converted into an impedance model by the inversion network. The resulting impedance model is then used to generate synthetic seismic records through the forward network, which is used to calculate the data misfit (i.e., $Loss_2$). It is important to note that we do not directly use the forward modeling operator to convert inverted impedance to seismic records. During the iterative optimization process, the recursive of traditional physical laws and wavelet convolution are computationally intensive. We employ a neural network to replace this process, thereby improving computational efficiency. The forward network is trained using synthetic data and can effectively characterize the relationship between impedance and seismic data. If the predicted impedance is close to the true impedance, the low-frequency background of the predicted impedance should be similar to that of the initial input impedance model. Therefore, we design an initial model loss term (i.e., $Loss_3$) to constrain the function space of the mapping, making it easier for the network to learn to predict impedance accurately. In addition, to ensure the coupling between predicted neighboring impedances, we design a lateral constraint term (i.e., $Loss_4$) for the neighboring traces.

The specific expression for the complete loss function is provided below:

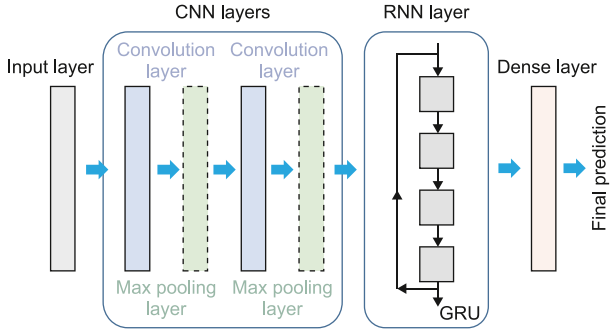

Fig. 3. Architecture of spatio-temporal neural network model.

$$\mathscr{L} = \underbrace{\lambda_1 \cdot ||\mathbf{m} - \mathscr{G}_\Theta(\mathbf{d}_l, \mathbf{m}_{0l})||_2^2}_{\mathscr{L}_1} + \underbrace{\lambda_2 \cdot ||\mathbf{d} - F(\mathscr{G}_\Theta(\mathbf{d}, \mathbf{m}_0))||_2^2}_{\mathscr{L}_2} + \underbrace{\lambda_3 \cdot ||\mathbf{m}_0 - s(\mathscr{G}_\Theta(\mathbf{d}, \mathbf{m}_0))||_2^2}_{\mathscr{L}_3} + \underbrace{\lambda_4 \cdot ||\mathbf{D} \cdot \mathscr{G}_\Theta(\mathbf{d}, \mathbf{m}_0)||_2^2}_{\mathscr{L}_4} \tag{2}$$

where $\mathscr{L}_1$ and $\mathscr{L}_2$ are the model misfit and data misfit terms, respectively, similar to $\mathscr{L}_1$ and $\mathscr{L}_2$ in Eq. (1). In our proposed method, we input both the initial impedance model and the seismic data into the network. $\mathbf{m}_{0l}$ represents the initial impedance model corresponding to the labelled data. $\mathbf{m}_0$ represents initial impedance model with or without labels. $\mathscr{L}_3$ is the initial model loss term. s is a smoothing operator that smooths the network predicted impedance so that it is close to the input impedance (i.e., $\mathbf{m}_0$). $\mathscr{L}_4$ is the lateral constraint term for the neighboring traces. $\mathbf{D}$ is a derivative matrix that ensures the lateral continuity of the prediction results, and its expression is shown in Eq. (3). λ is a weighting factor used to balance these four loss terms.

$$\mathbf{D} = [1 \quad -2 \quad 1] \odot \mathbf{I}_{n_t \times n_t} \tag{3}$$

where $\odot$ represents Kronecker tensor product. $\mathbf{I}$ is identity matrix. n_t represents the number of sampling points for a single trace. For more complex cases, lateral constraint operator can be constructed in conjunction with geo-statistical.

Feeding labelled and unlabelled training data into the designed network, the update of the network can be done using the loss

function shown in Eq. (2). The updated network can be used for subsequent prediction of the impedance model.

2.3. Spatio-temporal neural network

Network architecture is another key factor in the success of DL-based seismic inversion methods. Considering the spatio-temporal characteristics of seismic data and impedance models, this paper employs a spatio-temporal neural network (STNN) to validate the performance of the proposed method. The specific architecture of the STNN used for seismic inversion is presented in Fig. 3. The network consists of two main parts: CNN layers and a recurrent neural network (RNN) layer, where Gate Recurrent Unit (GRU) is used for the RNN layer. To enable the replication of the following numerical experiments, the detailed network parameters are listed below. The seismic data and the initial model are fed into the CNN layers, which consists of two convolutional layers. Each convolutional layer has 8 filters of size 5×1. The padding and dilation for each convolutional layer are configured as 2 and 1, respectively. To prevent overfitting, the first convolutional layer is followed by a dropout layer (dropout $= 0.1$). In addition, a ReLu activation function is applied after the first convolutional layer to introduce non-linearity into the mapping. After each convolutional layer, there is an option to add a pooling layer, depending on the specific requirements (e.g., accuracy and speed) of the task. The input passes through the CNN layers to complete feature extraction and is then fed into the RNN layer. The RNN layer is composed of a bidirectional GRU module, which introduces a bidirectional structure to more effectively capture dependencies in the sequence data. The number of features in the hidden state is set to 8, and the number of GRU layer is set to 2. The output of the RNN layer is then fed into a dense layer to generate the final prediction. The Adam optimizer is employed for network optimization during training, with a learning rate of 0.01 and an epoch of 1500. In the proposed method, both the inversion and forward networks use the same network structure.

3. Numerical examples

In this section, we seek to validate the effectiveness of the proposed method using synthetic data from the benchmark Marmousi model as well as a field dataset. The numerical experiments are performed using PyTorch as the backend on a PC with Windows 10, AMD Ryzen 7 5800X, and NVIDIA GeForce RTX 3080Ti. To demonstrate the advantages of the proposed method, we compare its results with those of traditional single-trace and multi-trace algorithms. For a fair comparison, all methods use the PGDL (i.e., physics-guided deep learning) strategy and have the same network structure. For the convenience of subsequent comparisons, the conventional PGDL-based single-trace inversion strategy is denoted as SPGDL, the conventional PGDL-based multi-trace inversion strategy is denoted as MPGDL, and the proposed laterally constrained multi-trace PGDL-based inversion strategy is denoted as LMPGDL. To quantitatively assess the inversion results, we employ the root mean square error (RMSE) defined as follows:

$$\mathrm{RMSE} = \sqrt{\frac{1}{N}\sum_{i=1}^{N}\left(Z_{\mathrm{p}}^{i} - \tilde{Z}_{\mathrm{p}}^{i}\right)^{2}} \tag{4}$$

where Z_{p} and $\tilde{Z}_{\mathrm{p}}$ denote true (or reference) impedance and inverted impedance, respectively. N represents the number of samples.

3.1. Synthetic example

As a benchmark model, the Marmousi model serves as a critical inversion example in the field of geophysical exploration. The known true geological parameters of the Marmousi model provide a standard platform for comparing the performance of different inversion algorithms, therefore, it is employed as an example to validate the effectiveness of the proposed method in this paper. Fig. 4(a) and (b) show the reference impedance model of Marmousi and its corresponding initial impedance model, respectively. The initial impedance model presented here is derived from the reference impedance model through the application of low-pass filtering techniques. In practical, such models can be easily generated using commercial software that incorporates known well-log and interpreted seismic horizon. It has a total size of 600 in the time direction and 3201 in the horizontal direction. The model is discretized with a time sampling interval of 2 ms. The reflection coefficients are calculated based on the reference impedance model using the post-stack forward equation, and then convolved with a zero-phase Ricker wavelet having a dominant frequency of 20 Hz to obtain a synthetic seismic record, as shown in Fig. 5(a). Adding Gaussian white noise to synthetic seismic records is a standard practice in seismic inversion to ensure that the algorithms being tested or developed are capable of handling the complexities and uncertainties inherent in real-world data. For this purpose, Gaussian noise is added to the noise-free seismic data (Fig. 5(a)) to obtain noisy seismic data with a signal-to-noise ratio (SNR) of 5, as illustrated in Fig. 5(b). This noisy seismic data will be used for subsequent inversion experiments. In this experiment, SPGDL, MPGDL, and LMPGDL all incorporate known physical laws, and all three methods use only one trace of labelled data-pairs (100th) during network training.

Fig. 6 shows the impedance inversion results obtained using the SPGDL method. For a more detailed observation and comparison, we provide a close-up view of the area indicated by the rectangular box in Fig. 6(a), as illustrated in Fig. 6(b). It is evident that by incorporating physical laws and low-frequency prior information, the prediction results reveal the subsurface strata well, even when only a single trace of labelled data is utilized for network training. However, SPGDL conducts training and prediction on a trace-by-trace basis, and the inversion results exhibit noticeable vertical stripes. The trace-by-trace inversion strategy fails to account for the interactions between adjacent traces and is susceptible to noise, which results in lateral discontinuities in the inversion. These discontinuities manifest as abrupt changes or inconsistencies across the reconstructed data, which can degrade the overall quality and reliability of the inverted results. The lateral discontinuities are inconsistent with the smooth and continuous nature of geological depositional processes. This inconsistency complicates subsequent interpretation and analysis, making it more challenging to derive accurate and meaningful insights from the data. Fig. 7 illustrates the reconstructed seismic record based on the SPGDL inversion results, along with its difference profile compared to the reference seismic record (Fig. 5(b)). Incorporating known physical laws into deep learning-based seismic inversion can ensure that the reconstructed seismic records are consistent with observed seismic data, thereby improving the interpretability and reliability of the inversion results.

Fig. 8 displays the impedance inversion results obtained using MPGDL, along with a local magnification for detailed examination. It can be observed that the lateral continuity of the inversion results for the MPGDL method is improved compared to those obtained using the SPGDL method. This enhancement in lateral continuity suggests that the MPGDL method is more effective in capturing the spatial relationships and reducing discontinuities,

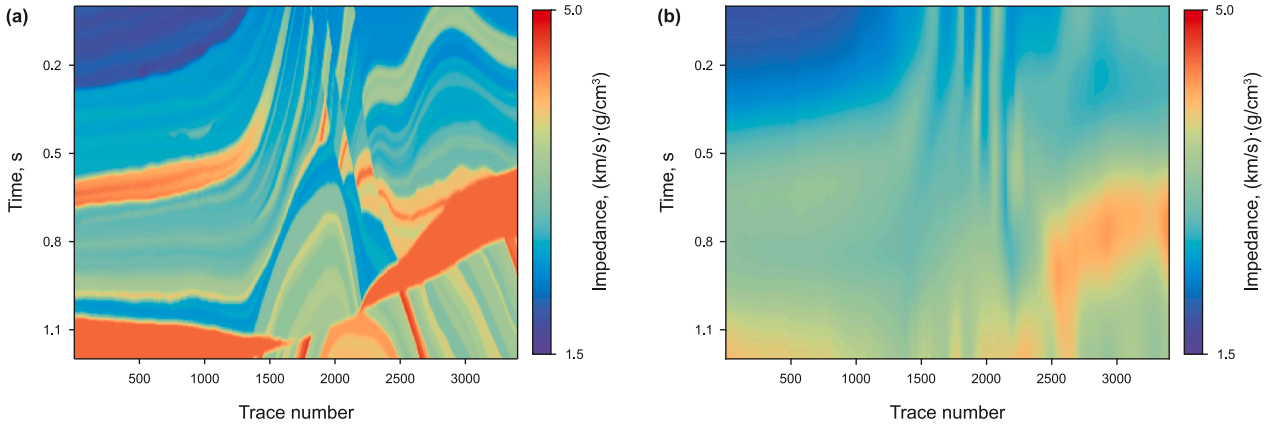

Fig. 4. Synthetic test of Marmousi model. **(a)** Reference impedance. **(b)** Initial impedance.

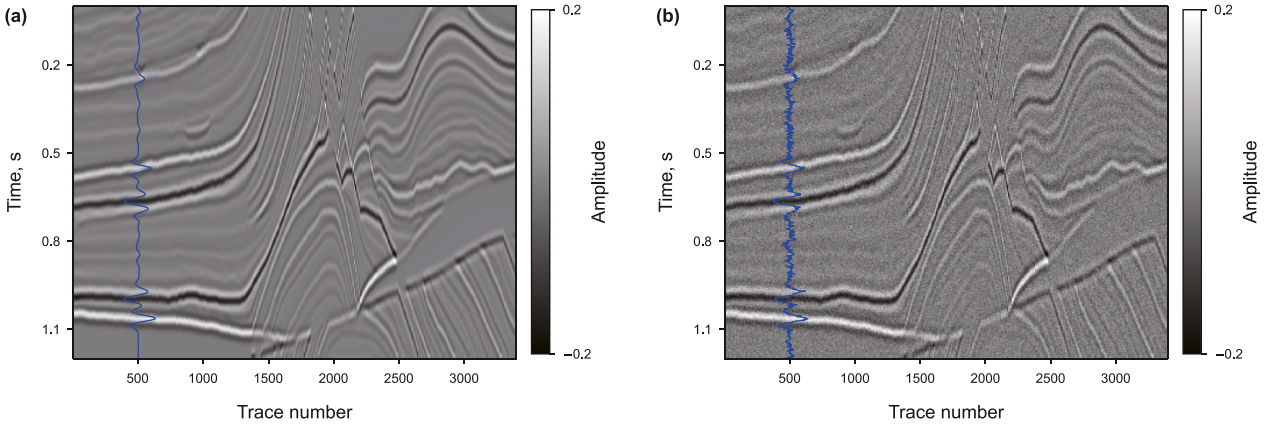

Fig. 5. Synthetic seismic data of Marmousi model. **(a)** Noise-free. **(b)** Noisy (SNR = 5).

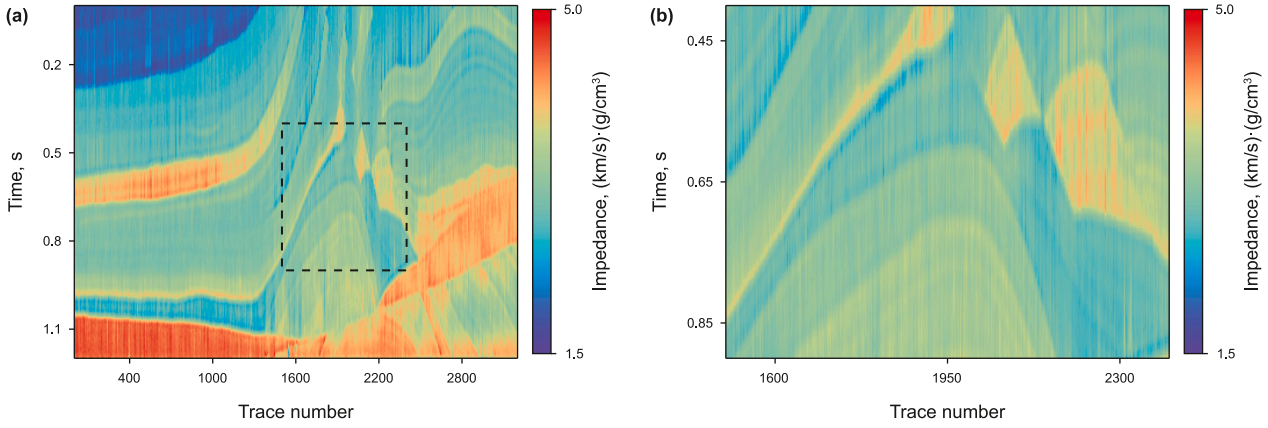

Fig. 6. The inverted results obtained using SPGDL. **(a)** Impedance. **(b)** A magnified view of the dashed rectangular area shown in (a).

leading to more coherent and reliable inversion outcomes. Fig. 9 illustrates the reconstructed seismic record based on the SPGDL inversion results, along with its difference profile compared to the reference seismic record (Fig. 5(b)). The reconstructed seismic record based on the inversion results shows a good match with the reference seismic record, indicating that the inversion process is effective in reproducing the observed data. Whether it is single-trace or multi-trace DL-based seismic inversion, the introduction of physical laws helps to ensure the physical consistency and validity of the inversion results. This integration enhances the reliability and interpretability of the reconstructed seismic data by aligning the predictions with known physical principles. The MPGDL method feeds multiple neighboring seismic traces into the network, allowing it to automatically learn similar features between these traces. This approach improves the lateral continuity of the prediction. However, the output of the MPGDL method

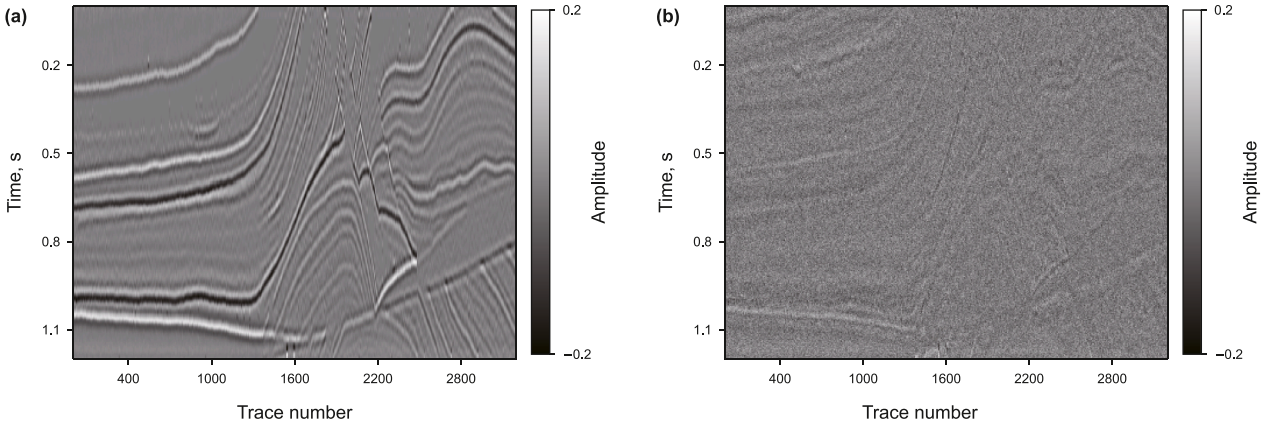

Fig. 7. **(a)** Reconstructed seismic records based on the inversion results of SPGDL. **(b)** The difference profile between the reconstructed seismic records (Fig. 7(a)) and the reference seismic records (Fig. 5(b)).

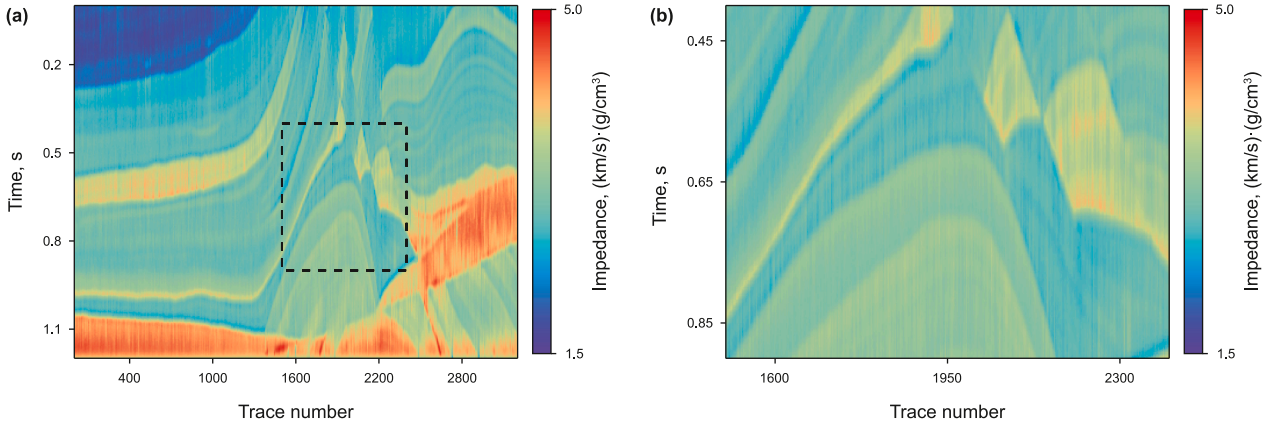

Fig. 8. The inverted results obtained using MPGDL. **(a)** Impedance. **(b)** A magnified view of the dashed rectangular area shown in (a).

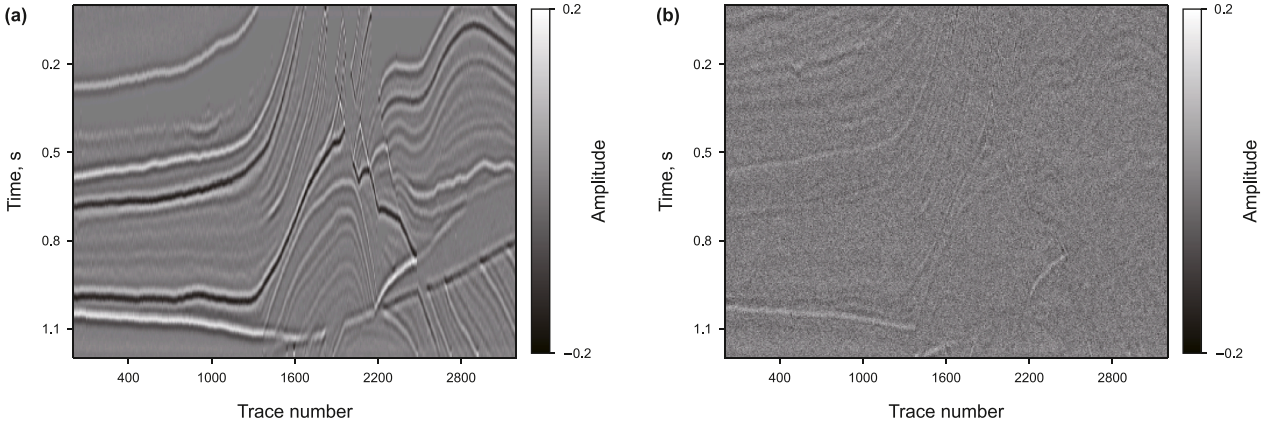

Fig. 9. **(a)** Reconstructed seismic records based on the inversion results of MPGDL. **(b)** The difference profile between the reconstructed seismic records (Fig. 9(a)) and the reference seismic records (Fig. 5(b)).

remains single-trace, which means it does not account for the coupling relationships between neighboring traces in the final output. Consequently, while the MPGDL method enhances continuity within individual traces, it still lacks the ability to fully capture the inter-trace dependencies that are crucial for a more comprehensive and coherent inversion result.

Based on the method MPGDL, LMPGDL introduces a coupling loss term between the outputs to ensure that the relationships between neighboring traces in the output results are maintained. This additional term helps to enforce the spatial coherence and inter-trace dependencies, leading to more physically consistent and reliable inversion results. Fig. 10 displays the impedance inversion results obtained using LMPGDL, along with a local magnification for detailed examination. It can be observed that the lateral continuity of the inversion results for the LMPGDL method is further improved compared to those obtained using the MPGDL method. In particular, the improvement in lateral continuity is more clearly evident in the local zoomed-in view, highlighting the

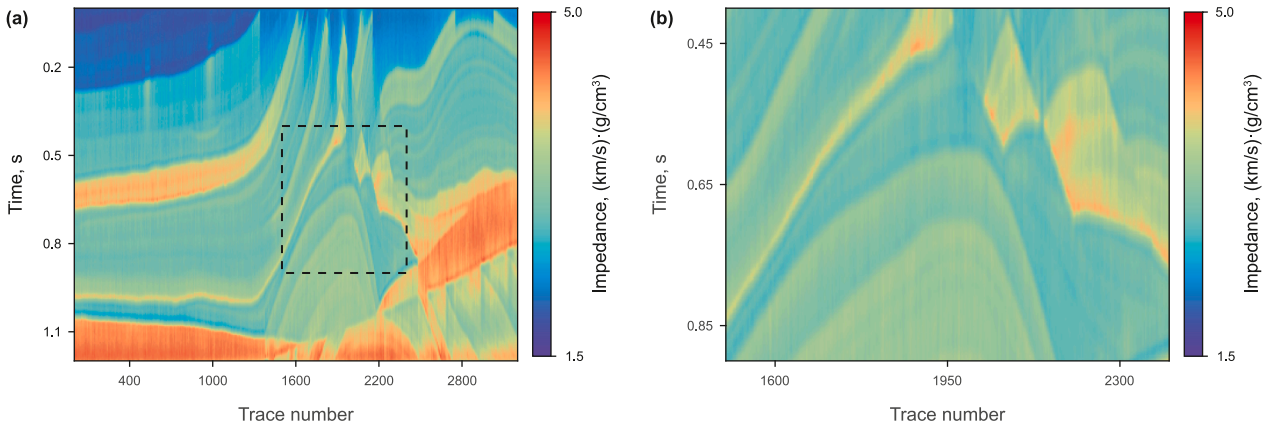

Fig. 10. The inverted results obtained using LMPGDL. **(a)** Impedance. **(b)** A magnified view of the dashed rectangular area shown in (a).

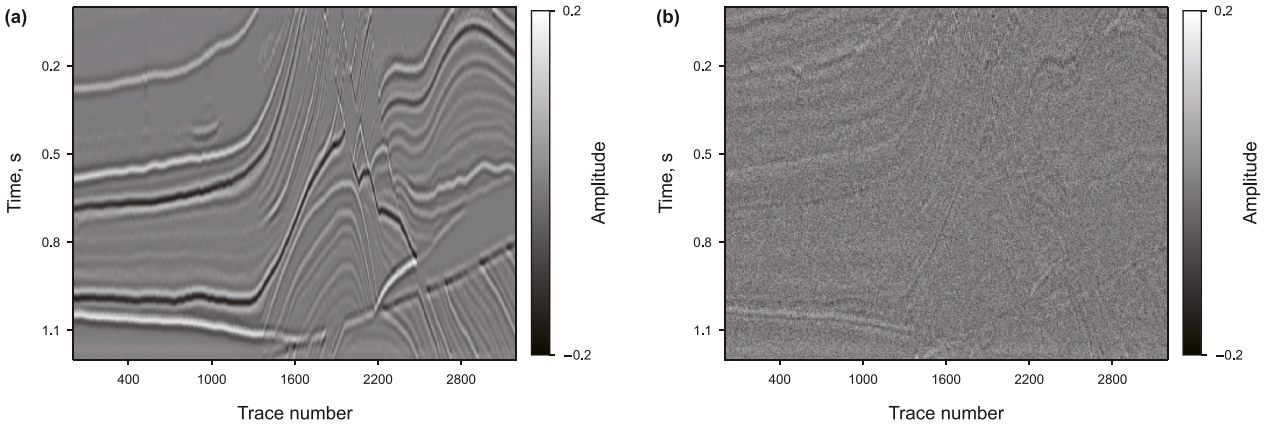

Fig. 11. **(a)** Reconstructed seismic records based on the inversion results of LMPGDL. **(b)** The difference profile between the reconstructed seismic records (Fig. 11(a)) and the reference seismic records (Fig. 5(b)).

enhanced spatial consistency of the inversion results. This enhancement indicates that the LMPGDL method is more effective in maintaining spatial consistency and reducing discontinuities in the inversion results. Similarly, the reconstructed seismic record based on the inversion results of LMPGDL can be matched with the reference seismic record, as shown in Fig. 11. This comparison shows that the LMPGDL method also produces results that are consistent with the observed data, which is consistent with the findings of the two previous methods.

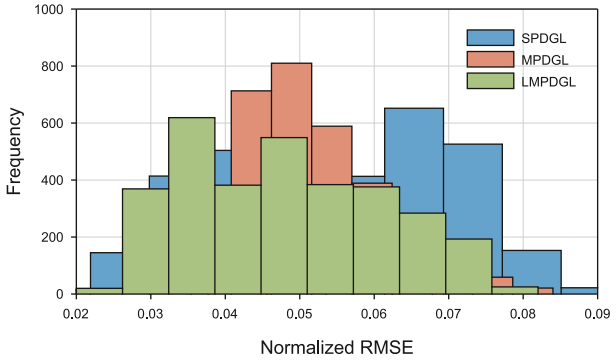

Fig. 12. Histogram of normalized root-mean-square error (RMSE) for the inversion results of SPGDL, MPGDL, and LMPGDL relative to the reference values.

The advantages and disadvantages of the three methods are qualitatively determined by comparing the results shown in Figs. 6, 8 and 10. To quantitatively assess the quality of the inversion results from the different methods, we calculate the normalized RMSE for each trace, comparing the inversion results with the reference values. Fig. 12 presents the histogram of the normalized RMSE for the inversion results of SPGDL, MPGDL, and LMPGDL relative to the reference values. The normalized RMSE of the MPGDL and LMPGDL inversion results are significantly smaller than those of the SPGDL inversion results. This quantitatively demonstrates the effectiveness of the multi-trace inversion strategy in improving the inversion results, highlighting its superiority in reducing errors compared to single-trace approaches. The normalized RMSE of the MPGDL and LMPGDL inversion results are similar, but LMPGDL has a higher proportion of smaller error values compared to MPGDL. Regarding computational efficiency, the SPGDL network requires approximately 150 s for training, while both MPGDL and LMPGDL demonstrate comparable training durations of around 230 s. Notably, all three methods exhibit negligible differences in prediction time (<1 s).

Figs. 13 and 14 illustrate the inversion results for a specific neighboring trace (749th and 750th) using the three methods. It can be seen that the inversion results of all the three methods can be in good agreement with the reference well curves. As can be seen from any of the figures, the inversion results of all three methods show good agreement with the reference well curves, indicating their effectiveness in reproducing the observed data.

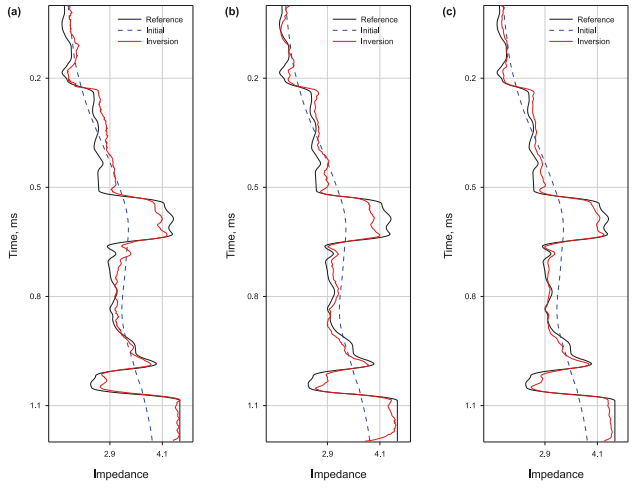

Fig. 13. Comparison of single-trace (750th) inversion results for **(a)** SPGDL, **(b)** MPGDL and **(c)** LMPGDL.

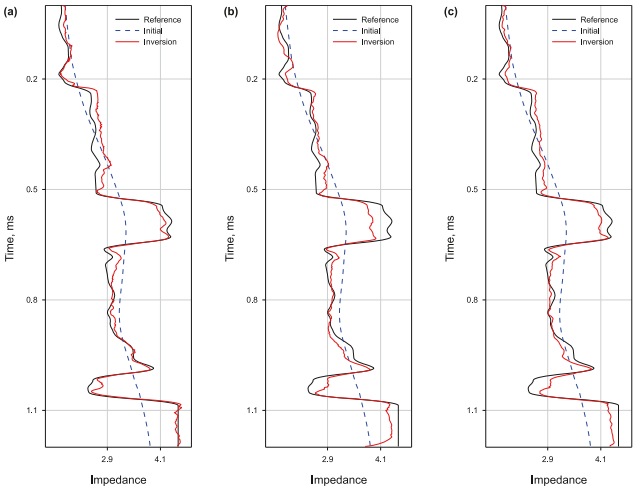

Fig. 14. Comparison of single-trace (749th) inversion results for **(a)** SPGDL, **(b)** MPGDL and **(c)** LMPGDL.

However, comparing the two figures, it is evident that the inversion results of MPGDL and LMPGDL exhibit better stability compared to SPGDL. The unstable single-trace inversion results exhibit lateral discontinuities (i.e., vertical stripes), when combined into a 2D profile, as shown in Fig. 6. The multi-trace inversion strategy ensures that the coupling relationships between neighboring traces are maintained, leading to better lateral continuity in the 2D profile, as shown in Figs. 8 and 10.

3.2. Field data example

The synthetic data test demonstrates the effectiveness of the proposed method. Based on these promising results, we further apply the method to real data to validate its practical applicability and robustness. The study area is located in the Lower Congo Basin, which is one of the series of passive continental margin basins along the West African coast. It is a superimposed basin formed by the coexistence of continental rift structures and passive margin basins. The reservoirs in this basin are composed of turbidite sand bodies from the Oligocene and Miocene strata. Fig. 15(a) illustrates the crossing-well seismic profile used for testing. The seismic data

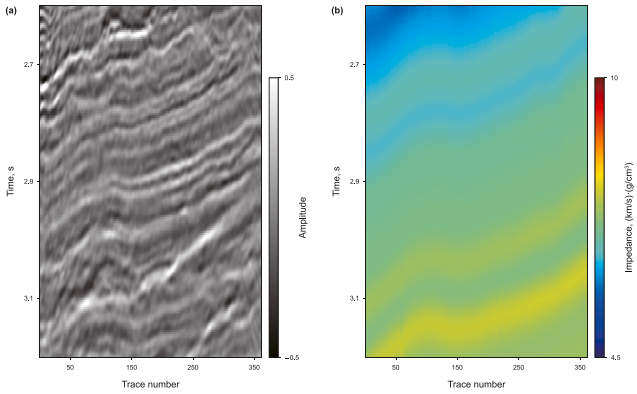

Fig. 15. Real case test. **(a)** Crossing-well seismic profile. **(b)** Initial impedance model.

have been preprocessed to enhance their quality and reliability through denoising and amplitude calibration. In this test, two wells are included, one well-log is used for network training, while the other well-log is used for blind well validation. The low-frequency initial model, obtained using commercial software based on the known well-log data and picked seismic horizons, is shown in Fig. 15(b). A combination of well data and unlabelled data is used for network training, and the trained network is then used for impedance prediction across the profile.

Fig. 16 shows the impedance inversion results obtained using the SPGDL method. For a more detailed observation and comparison, a close-up view of the area indicated by the rectangular box in Fig. 16(a) is provided in Fig. 16(b). The resolution of the inversion results is significantly improved compared to the initial model, demonstrating the enhanced clarity and detail provided by the inversion process. However, due to the influence of noise in the seismic data, the inversion results obtained using the SPGDL method exhibit obvious fluctuations, leading to weak lateral continuity. The SPGDL method performs the inversion on a trace-by-trace basis and cannot account for the coupling between neighboring seismic traces. This makes the method sensitive to noise, leading to reduced lateral continuity and incoherent inversion results. The magnified local image (Fig. 16(b)) shows the details more clearly, revealing the presence of noise blocks laterally between the same strata. This is inconsistent with the general process of stratigraphic deposition. Fig. 17 illustrates the reconstructed seismic record based on the SPGDL inversion results, along with a local magnification to show the details more clearly. The reconstructed seismic records (Fig. 17(a)) are in good

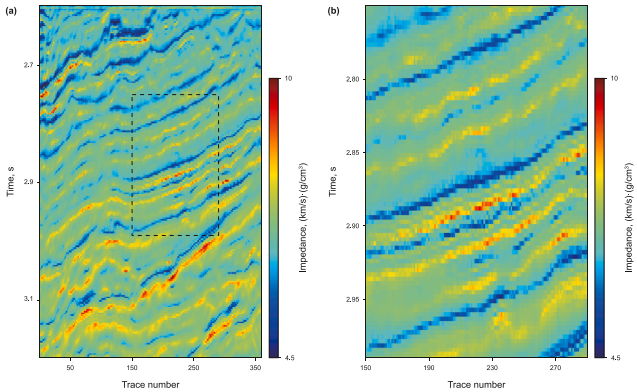

Fig. 16. The inverted results obtained using SPGDL. **(a)** Impedance. **(b)** A magnified view of the dashed rectangular area shown in (a).

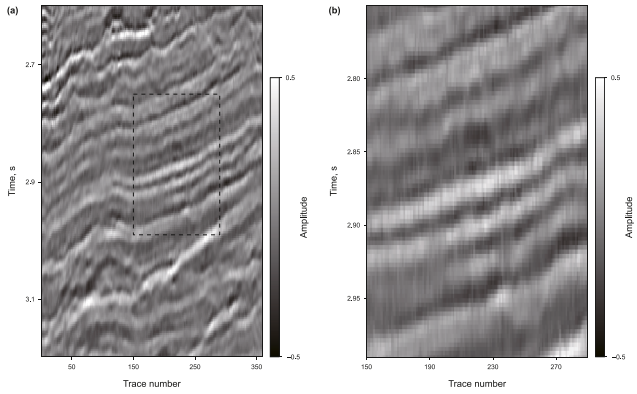

Fig. 17. **(a)** Reconstructed seismic records based on the inversion results of SPGDL. **(b)** A magnified view of the dashed rectangular area shown in (a).

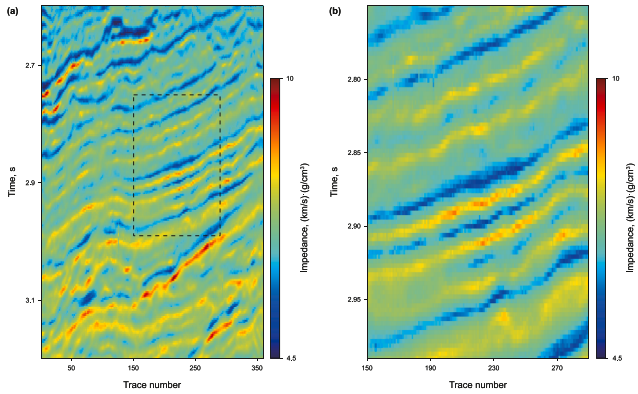

Fig. 18. The inverted results obtained using MPGDL. **(a)** Impedance. **(b)** A magnified view of the dashed rectangular area shown in (a).

agreement with the observed seismic data (Fig. 15(a)), proving that the introduction of physical laws in DL-based seismic inversion methods is effective. The lateral continuity of the inversion results from the SPGDL method is poor, and consequently, the lateral continuity of the seismic record reconstructed based on these results is also poor, as shown in Fig. 17(b).

Figs. 18–21 show the inversion results for the MPGDL and LMPGDL methods, along with their corresponding reconstructed seismic records. It can be seen that the lateral continuity of the inversion results using the multi-trace strategy (i.e., MPGDL and

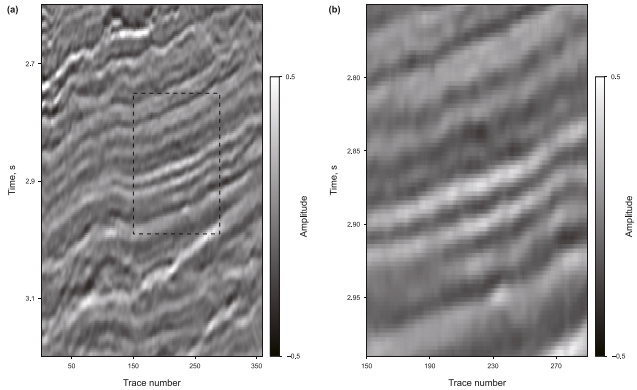

Fig. 19. **(a)** Reconstructed seismic records based on the inversion results of MPGDL. **(b)** A magnified view of the dashed rectangular area shown in (a).

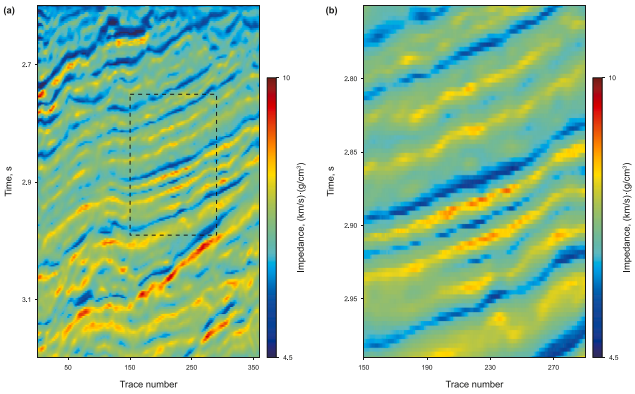

Fig. 20. The inverted results obtained using LMPGDL. **(a)** Impedance. **(b)** A magnified view of the dashed rectangular area shown in (a).

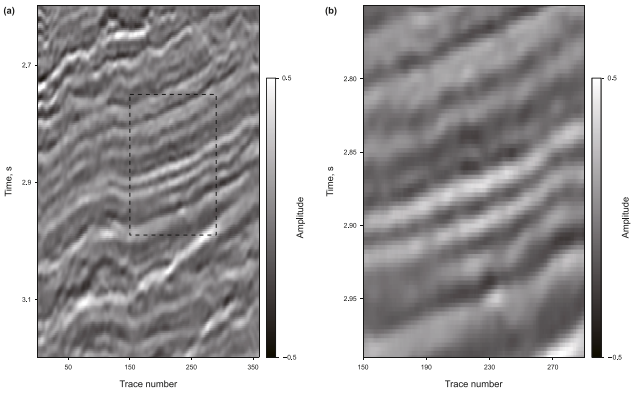

Fig. 21. **(a)** Reconstructed seismic records based on the inversion results of LMPGDL. **(b)** A magnified view of the dashed rectangular area shown in (a).

LMPGDL) is significantly improved compared to that of the single-trace strategy (i.e., SPGDL). This enhancement demonstrates the effectiveness of the multi-trace approach in maintaining spatial coherence and reducing discontinuities. The local zoomed-in view of the MPGDL and LMPGDL inversion results clearly shows a more natural and rational stratigraphic pattern. However, the resolution of the inversion results using the multi-

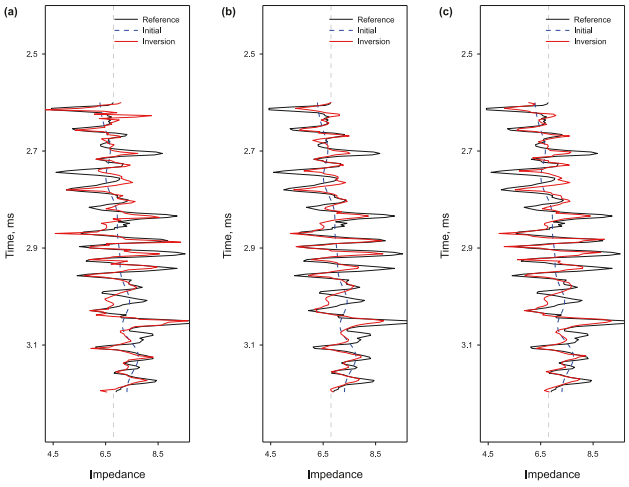

Fig. 22. Comparison of inversion results of different methods with blind well-log. **(a)** SPGDL, **(b)** MPGDL, **(c)** LMPGDL.

Table 1
The normalized-root-mean-square error (RMSE) between the true and the inverted impedance using SPGDL, MPGDL, and LMPGDL for the field data (blind well-log).

	MGNN	PGNN	PMGNN
RMSE	0.0482	0.0456	**0.0445**

trace strategy (i.e., MPGDL and LMPGDL) is slightly reduced compared to that of the single-trace strategy (i.e., SPGDL). Both MPGDL and LMPGDL methods take into account the laws of physics, and the reconstructed seismic records based on their inversion results are in good agreement with the observed seismic records. As the lateral continuity of the inversion results is improved, the lateral continuity of the seismic records obtained from them is also enhanced, as shown in Figs. 19(b) and 21(b). By considering the coupling relationship between neighboring traces, the lateral continuity of the inversion results and their reconstructed seismic records of LMPGDL is superior when compared to the inversion results and reconstructed seismic records of MPGDL.

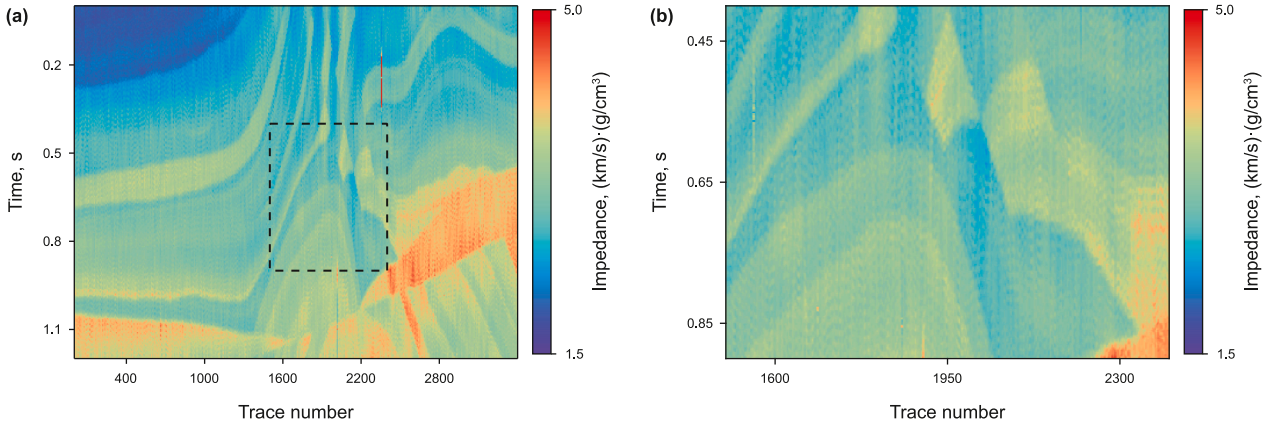

Fig. 23. The inverted results obtained using model-base method with lateral constraints. **(a)** Impedance. **(b)** A magnified view of the dashed rectangular area shown in (a).

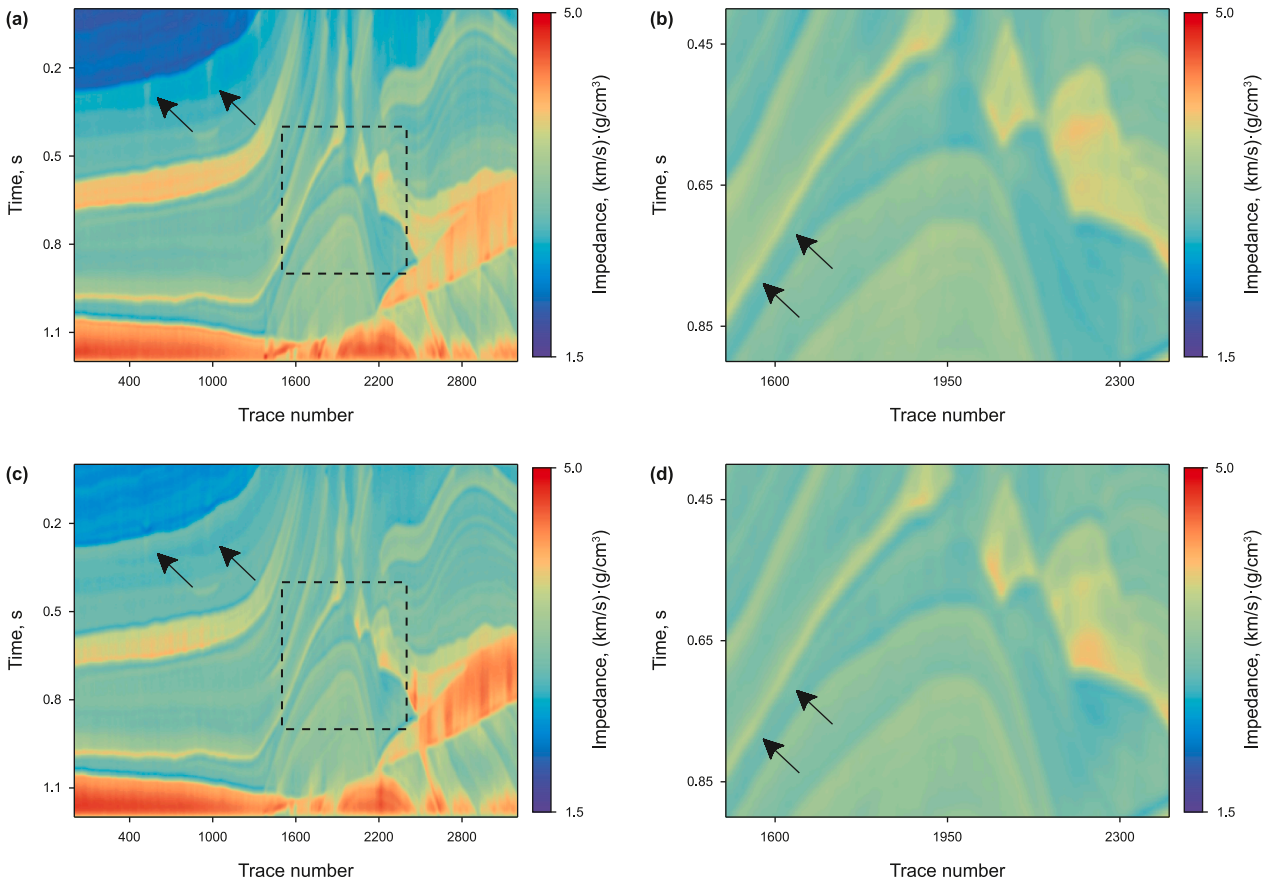

Fig. 24. The inverted results obtained using LMPGDL with different number of adjacent traces. **(a)** 7, **(c)** 11. The second column **(b)** and **(d)** shows a localized zoomed-in display of the results from the first column.

Subsequently, we compare the inversion results with the blind well-log data to further verify the validity of the proposed method, as shown in Fig. 22. Blind well-log data, which is not involved in the training process of the network at any stage, can be better used as a comparison group to validate the method. From Fig. 22, we observe that the inversion results of MPGDL and LMPGDL exhibit better stability and a closer match to the reference well-log curve. However, the SPGDL inversion results are significantly oscillatory and exhibit lateral discontinuities when spliced into 2D profiles, as shown in Fig. 16. To quantitatively assess the quality of the inversion results, we calculate the normalized RMSE between the inversion results and the reference well-log curve (i.e., blind well). Table 1 lists the normalized RMSEs between the blind well-log data and the inverted results of SPGDL, MPGDL, and LMPGDL. MPGDL and LMPGDL have a smaller normalized RMSE, which proves the effectiveness of the multi-trace inversion strategy in improving the inversion results. The normalized RMSE of the MPGDL and LMPGDL inversion results are similar, but LMPGDL is optimal.

4. Discussion

Deep learning has demonstrated impressive success across various fields, and it has also introduced innovative approaches to seismic inversion, yielding highly encouraging outcomes. However, the challenge of applying deep learning methods in a more physically meaningful manner to seismic inversion, in order to achieve superior results, remains an actively explored and evolving research direction for scholars. In its nascent stages, seismic inversion using deep learning is predominantly data-driven, exhibiting a strong reliance on large volumes of training data. Over time, the field has progressed towards the development of semi-supervised inversion methodologies that integrate physical laws and geological constraints (Biswas et al., 2019; Zhang et al., 2021c). This advancement not only imbues seismic inversion with a more robust physical interpretation but also effectively reduces the dependency on extensive training datasets.

Taking into account the lateral continuity of adjacent traces in the subsurface, this paper proposes a multi-trace inversion approach built upon prior research in physics-guided deep learning seismic inversion. This method effectively addresses the limitation of lateral discontinuity inherent in trace-by-trace inversion results. The multi-trace strategy comprises two methodologies. The first methodology involves utilizing multi-trace seismic data as input, enabling the network to autonomously discern correlations among adjacent traces. The second methodology focuses on the development of a tailored loss function designed to enforce lateral continuity between neighboring traces in the output. Experimental results indicate that the second methodology is significantly more effective in enhancing the lateral continuity of inversion outcomes. The second method was inspired by the work of Hamid and Pidlisecky (2015). To further demonstrate the advantages of the proposed approach, an inversion test based on a model-driven multi-trace strategy (Hamid and Pidlisecky, 2015) is conducted under the same input data conditions. The results are shown in Fig. 23. It can be observed that the inversion results of LMPGDL reveal more geological details compared to those obtained from the model-driven inversion method. Furthermore, the inversion results of LMPGDL are closer to the reference model. In addition to the visual comparison, the model-driven method take approximately 980 s to complete the inversion task in this experiment, which is significantly higher than the time cost of the deep learning-based inversion method.

The multi-trace inversion strategy yields results with enhanced lateral continuity compared to the trace-by-trace inversion approach, but this is achieved at the expense of the vertical resolution. While increasing the number of adjacent traces can further increase lateral continuity, this also leads to details being blurred out, as shown in Fig. 24. And the network training time increases from 230 s to 590 s as the number of adjacent traces increases from 3 to 11. In addition, the proposed method only considers the similarity in the horizontal direction of neighboring traces, which leads to the details of steep strata segments being blurred out. To further improve the vertical resolution of the inversion results, adding sparse constraints (Zhang et al., 2012) or introducing stratigraphic dip information (Zhang et al., 2021b) might be good choices.

5. Conclusion

In this paper, we propose a laterally constrained multi-trace deep learning-based seismic inversion method to enhance the continuity and geological reliability of the inversion results. The method utilizes adjacent multi-trace seismic data as network inputs and incorporates a multi-trace coupling constraints, thereby enhancing the lateral continuity of the inversion results. The LMPGDL method is first applied to the Marmousi model and compared with SPGDL and MPGDL. The results indicate that LMPGDL obtain more continuous results in the lateral compared to the other methods. All three methods incorporate physical laws, and the reconstructed seismic records based on their inversion results match the observed seismic data well. The reconstruction of seismic records is influenced by the inversion results. The inversion results from the SPGDL method suffer from insufficient lateral continuity, resulting in correspondingly poor continuity in the reconstructed seismic records. Both the inversion results and the reconstructed seismic records demonstrate that the multi-trace strategy improves the lateral continuity of the results compared to the single-trace strategy, making the results more consistent with geological patterns. It is worth noting that achieving optimal results requires a balanced consideration of both lateral continuity and vertical resolution. Experiments from synthetic and actual data qualitatively and quantitatively demonstrate that the proposed method is optimal.

CRediT authorship contribution statement

Jian Zhang: Writing – original draft, Methodology, Formal analysis, Conceptualization. **Yi-Ran Xue:** Validation, Investigation. **Xiao-Yan Zhao:** Writing – review & editing, Visualization, Methodology. **Jing-Ye Li:** Writing – review & editing, Supervision, Project administration.

Data availability

Model data and code associated with this research are available and can be obtained by contacting the corresponding author.

Declaration of interests

The authors declare that they have no known competing financial interests or personal relationships that could have appeared to influence the work reported in this paper.

Acknowledgements

This work was supported in part by the National Natural Science Foundation of China under Grant 42204108 and 42530806, in part by the Sichuan Science and Technology Program under Grant 2026NSFSC0235.

References

Ahmed, N., Waldemar Weibull, W., Grana, D., Bhakta, T.J., 2024. Constrained nonlinear amplitude-variation-with-offset inversion for reservoir dynamic changes estimation from time-lapse seismic data. Geophysics 89 (1), R1–R15. https://doi.org/10.1190/geo2022-0750.1.

Aleardi, M., Salusti, A.J., 2021. Elastic prestack seismic inversion through discrete cosine transform reparameterization and convolutional neural networks. Geophysics 86 (1), R129–R146. https://doi.org/10.1190/geo2020-0313.1.

Biswas, R., Sen, M., Das, V., Mukerji, T., 2019. Prestack and poststack inversion using a physics-guided convolutional neural network. Interpretation 7 (3), SE161–SE174. https://doi.org/10.1190/INT-2018-0236.1.

Bosch, M., Mukerji, T., Gonzalez, E.F.J., 2010. Seismic inversion for reservoir properties combining statistical rock physics and geostatistics: A review. Geophysics 75 (5), 75A165–175A176. https://doi.org/10.1190/1.3478209.

Cao, D., Su, Y., Cui, R.J., 2022. Multi-parameter pre-stack seismic inversion based on deep learning with sparse reflection coefficient constraints. J. Petrol. Sci. Eng. 209, 109836. https://doi.org/10.1016/j.petrol.2021.109836.

Chen, H., Li, J., Innanen, K.A.J., 2020. Nonlinear inversion of seismic amplitude variation with offset for an effective stress parameter. Geophysics 85 (4), R299–R311. https://doi.org/10.1190/geo2019-0154.1.

Chen, H., Wu, B., Sacchi, M.D., Wang, Z., Gao, J.J., 2024. Multidimensional petrophysical seismic inversion based on knowledge-driven semi-supervised deep learning. IEEE Trans. Geosci. Rem. Sens. 62, 5927215. https://doi.org/10.1109/TGRS.2024.3460184.

Das, V., Pollack, A., Wollner, U., Mukerji, T.J., 2019. Convolutional neural network for seismic impedance inversion. Geophysics 84 (6), R869–R880. https://doi.org/10.1190/geo2018-0838.1.

Delépine, N., Clochard, V., Labat, K., Ricarte, P.J., 2011. Post-stack stratigraphic inversion workflow applied to carbon dioxide storage: Application to the saline aquifer of Sleipner field. Geophys. Prospect. 59 (1), 132–144. https://doi.org/10.1111/j.1365-2478.2010.00905.x.

Dodda, V.C., Kuruguntla, L., Mandpura, A.K., Elumalai, K., Sen, M.K.J., 2023. Deep convolutional neural network with attention module for seismic impedance inversion. IEEE J. Sel. Top. Appl. Earth Obs. Rem. Sens. 16, 8076–8086. https://doi.org/10.1109/JSTARS.2023.3308751.

Fernandes, F.J.D., de Oliveira Neto, E.R., Teixeira, L., Freire, A.F.M., Lupinacci, W.M.J., 2024. Cycle-consistent convolutional neural network for seismic impedance inversion: An application for high-resolution characterization of turbidites reservoirs. Geoenergy Sci. Eng. 235, 212709. https://doi.org/10.1016/j.geoen.2024.212709.

Gao, Y., Li, H., Li, G., Wei, P., Zhang, H.J., 2024. Deep learning for high-resolution multichannel seismic impedance inversion. Geophysics 89 (1), WA323–WA335. https://doi.org/10.1190/geo2023-0096.1.

Gao, Z., Li, C., Liu, N., Pan, Z., Gao, J., Xu, Z.J., 2020. Large-dimensional seismic inversion using global optimization with autoencoder-based model dimensionality reduction. IEEE Trans. Geosci. Rem. Sens. 59 (2), 1718–1732. https://doi.org/10.1109/TGRS.2020.2998035.

Grana, D., Azevedo, L., De Figueiredo, L., Connolly, P., Mukerji, T.J., 2022. Probabilistic inversion of seismic data for reservoir petrophysical characterization: review and examples. Geophysics 87 (5), M199–M216. https://doi.org/10.1190/geo2021-0776.1.

Guo, R., Zhang, J., Liu, D., Zhang, Y., Zhang, D., 2019. Application of bi-directional long short-term memory recurrent neural network for seismic impedance inversion. In: 81st EAGE Conference and Exhibition 2019. https://doi.org/10.3997/2214-4609.201901386.

Ha, T., Marfurt, K.J., 2017. The value of constrained conjugate-gradient least-squares migration in seismic inversion: Application to a fractured-basement play, Texas Panhandle. Interpretation 5 (3), SN13–SN23. https://doi.org/10.1190/INT-2016-0240.1.

Hamid, H., Pidlisecky, A.J., 2015. Multitrace impedance inversion with lateral constraints. Geophysics 80 (6), M101–M111. https://doi.org/10.1190/geo2014-0546.1.

Huang, G., Chen, X., Luo, C., Chen, Y.J., 2020. Pre-stack seismic inversion based on ℓ_{1-2}-norm regularized logarithmic absolute misfit function. Geophys. Prospect. 68 (8), 2419–2443. https://doi.org/10.1111/1365-2478.13012.

Lin, Y., Theiler, J., Wohlberg, B.J., 2023. Physics-guided data-driven seismic inversion: recent progress and future opportunities in full-waveform inversion. IEEE Signal Process. Mag. 40 (1), 115–133. https://doi.org/10.1109/MSP.2022.3217658.

Liu, B., Jiang, P., Wang, Q., Ren, Y., Yang, S., Cohn, A.G.J., 2023a. Physics-driven self-supervised learning system for seismic velocity inversion. Geophysics 88 (2), R145–R161. https://doi.org/10.1190/geo2021-0302.1.

Liu, Z., Chen, X., Li, J., Hou, S., Li, Z., Liu, G.J., 2023b. Robust weakly supervised learning pre-stack multi-trace seismic inversion. IEEE Trans. Geosci. Rem. Sens. 62, 5903811. https://doi.org/10.1109/TGRS.2023.3302352.

Mousavi, S.M., Beroza, G.C.J., 2022. Deep-learning seismology. Science 377 (6607), eabm4470. https://doi.org/10.1126/science.abm4470.

Mustafa, A., AlRegib, G., 2020. Joint learning for seismic inversion: An acoustic impedance estimation case study. In: SEG Technical Program Expanded Abstracts 2020, pp 1686–1690. https://doi.org/10.1190/segam2020-3428378.1.

Pendrel, J.J., 2001. Seismic inversion—The best tool for reservoir characterization. CSEG Rec. 26 (1), 18–24.

Röth, G., Tarantola, A.J., 1994. Neural networks and inversion of seismic data. J. Geophys. Res. Solid Earth 99 (B4), 6753–6768. https://doi.org/10.1029/93JB01563.

Shi, Y., Yu, B., Zhou, H., Cao, Y., Wang, W., Wang, N., 2024. FMG_INV, a fast multi-Gaussian inversion method integrating well-log and seismic data. IEEE Trans. Geosci. Rem. Sens. 62, 4503112. https://doi.org/10.1109/TGRS.2024.3351207.

Song, L., Yin, X., Zong, Z., Jiang, M.J., 2022. Semi-supervised learning seismic inversion based on spatio-temporal sequence residual modeling neural network. J. Petrol. Sci. Eng. 208, 109549. https://doi.org/10.1016/j.petrol.2021.109549.

Veeken, P., Da Silva, M., 2004. Seismic inversion methods and some of their constraints. First Break 22 (6), 47–70. https://doi.org/10.3997/1365-2397.2004011.

Wang, P., Cui, Y.-A., Chen, X., Pan, X., Liu, J.J., 2022. Analysis and application of the sparse prior in probabilistic prediction of elastic parameters. IEEE Trans. Geosci. Rem. Sens. 60, 1–9. https://doi.org/10.1109/TGRS.2022.3181175.

Wu, X., Yan, S., Bi, Z., Zhang, S., Si, H.J., 2021. Deep learning for multidimensional seismic impedance inversion. Geophysics 86 (5), R735–R745. https://doi.org/10.1190/geo2020-0564.1.

Zhang, H., Yang, P., Liu, Y., Luo, Y., Xu, J.J., 2021a. Deep learning-based low-frequency extrapolation and impedance inversion of seismic data. IEEE Geosci. Rem. Sens. Lett. 19, 1–5. https://doi.org/10.1109/LGRS.2021.3123955.

Zhang, J., Li, J., Chen, X., Li, Y., 2021b. Geological structure-guided hybrid MCMC and Bayesian linearized inversion methodology. J. Petrol. Sci. Eng. 199, 108296. https://doi.org/10.1016/j.petrol.2020.108296.

Zhang, J., Zhao, X., Chen, Y., Sun, H., 2023. Domain knowledge-guided data-driven prestack seismic inversion using deep learning. Geophysics 88 (2), M31–M47. https://doi.org/10.1190/geo2021-0560.1.

Zhang, J., Sun, H., Yuan, W., Yang, C., Xue, Y., 2022. Post-stack impedance inversion based on spatio-temporal neural network. IEEE Geosci. Rem. Sens. Lett. 19, 1–5. https://doi.org/10.1109/LGRS.2022.3227071.

Zhang, J., Li, J., Chen, X., Li, Y., Huang, G., Chen, Y., 2021c. Robust deep learning seismic inversion with a priori initial model constraint. Geophys. J. Int. 225 (3), 2001–2019. https://doi.org/10.1093/gji/ggab074.

Zhang, R., Sen, M.K., Phan, S., Srinivasan, S., 2012. Stochastic and deterministic seismic inversion methods for thin-bed resolution. J. Geophys. Eng. 9 (5), 611–618. https://doi.org/10.1088/1742-2132/9/5/611.

Zheng, Y., Zhang, Q., Yusifov, A., Shi, Y., 2019. Applications of supervised deep learning for seismic interpretation and inversion. Lead. Edge 38 (7), 526–533. https://doi.org/10.1190/tle38070526.1.

Zhou, D., Yin, X., Zong, Z., 2019. Multi-trace basis-pursuit seismic inversion for resolution enhancement. Geophys. Prospect. 67 (3), 519–531. https://doi.org/10.1111/1365-2478.12752.

Zhou, L., Chen, Z.-C., Li, J.-Y., Chen, X.-H., Liu, X.-Y., Liao, J.-P.J., 2020. Nonlinear amplitude versus angle inversion for transversely isotropic media with vertical symmetry axis using new weak anisotropy approximation equations. Pet. Sci. 17, 628–644. https://doi.org/10.1007/s12182-020-00445-x.

Zou, B., Wang, Y., Chen, T., Liang, J., Yu, G., Hu, G.J., 2023. The domain adversarial and spatial fusion semi-supervised seismic impedance inversion. IEEE Trans. Geosci. Rem. Sens. 62, 1–15. https://doi.org/10.1109/TGRS.2023.3336392.